Impact-parameter analysis of elastic scattering from 50 to 175 GeV/c†

D. S. Ayres and R. Diebold
Argonne National Laboratory, Argonne, Illinois 60439

D. Cutts, R. E. Lanou, L. J. Levinson, and J. T. Massimo
Brown University, Providence, Rhode Island 02912

J. Litt* and R. Meunier‡
CERN, Geneva, Switzerland

M. Sogard,§ B. Gittelman, and E. C. Loh‖
Cornell University, Ithaca, New York 14850

A. E. Brenner, J. E. Elias, and G. Mikenberg
Fermi National Accelerator Laboratory, Batavia, Illinois 60510

L. Guerriero, P. Lavopa, G. Maggi, C. DeMarzo, F. Posa, G. Selvaggi, P. Spinelli, and F. Waldner
Istituto Nazionale di Fisica Nucleare, Sezione di Bari, Italy

D. S. Barton, J. Butler,¶ J. Fines, J. I. Friedman, H. W. Kendall, B. Nelson, L. Rosenson, and R. Verdier
Massachusetts Institute of Technology, Cambridge, Massachusetts 02139

B. Gottschalk
Northeastern University, Boston, Massachusetts 02115

R. L. Anderson, D. Gustavson, K. Rich, D. M. Ritson, and G. A. Weitsch**
Stanford Linear Accelerator Center, Stanford, California 94305

(Received 2 August 1976)

Impact-parameter representations of elastic differential cross sections for the processes $\pi^{\pm}p$, $K^{\pm}p$, pp, and $\bar{p}p$ at incident energies from 50 GeV to 175 GeV and in the $-t$ range 0.03–0.75 GeV^2 are presented. The meson-baryon interactions are found to be 20% more transparent than the baryon-baryon interaction, and to have an interaction radius which is 6% smaller. The increase in the p-p total cross section as a function of energy is shown to come primarily from an increase in the p-p interaction radius, while in the K^+p case an increase is seen in both the central opacity and the interaction radius.

I. INTRODUCTION

With the discovery of the dip at $t \approx -1.4$ GeV^2 in pp elastic scattering[1] and the measurements of the real part of the elastic amplitude at $t = 0$ (Ref. 2) in the Fermilab–CERN-ISR energy range, it became apparent that the elastic scattering amplitude can be considered, to a good approximation, to be purely imaginary at high energies. This fact has enabled several authors[3-6] to perform a transformation of the pp elastic amplitude to impact-parameter space, and further, to obtain the total and inelastic cross sections as a function of the impact parameter making use of the fact that the S-matrix is diagonal in impact-parameter space. The observed increase in the inelastic and total cross sections as a function of energy for pp collisions was found to be peripheral and centered at an impact parameter, b, of approximately 1 fermi.[3-6] The Pumplin bound[7] for inelastic diffraction was also obtained, and the implications were that inelastic diffraction is more peripheral than the elastic process.

This paper presents the results of an impact-parameter analysis of the elastic reactions $\pi^{\pm}p$, $K^{\pm}p$, pp, and $\bar{p}p$ for incident momenta from 50 to 175 GeV/c and for $-t$ in the range 0.03 to 0.75 GeV^2, obtained with the Fermilab Single Arm Spectrometer in the $M6E$ beam line, that has been described in a previous publication.[8] Similar analyses have been done on preliminary data[9] and the results are consistent with those included in this publication. In the next section a discussion of the method used to transform the elastic data to impact-parameter space and the error calculation for this procedure are presented. In Sec. III the general characteristics of the different reactions in impact-parameter space, including their energy dependence, are discussed. In Sec. IV the observed increase in the total and inelastic K^+p and pp cross sections is correlated with changes in the impact-parameter distributions. Section V con-

tains results on the upper limits for inelastic diffraction as a function of the impact parameter. The peripherality of ω exchange has been discussed in connection with low-energy $K^{\pm}p$ data,[10] and in Sec. VI those conclusions are extended to the Fermilab energy range. In Sec. VII the hadronic matter distributions for π, K, and p as calculated using the Chou-Yang model are compared with electromagnetic form-factor measurements. In Sec. VIII comparisons with quark-model predictions as viewed in impact-parameter space are shown. Conclusions are presented in the final section.

II. ELASTIC CROSS SECTIONS AND TRANSFORMATION METHOD

The results from the Fermilab Single Arm Spectrometer on the differential elastic cross sections for the processes $\pi^{\pm}p$, $K^{\pm}p$, pp, and $\bar{p}p$ have been published previously,[8] and can all be satisfactorily fitted by the parametrization

$$d\sigma/dt = Ae^{Bt+Ct^2} \tag{1}$$

for $-t \leq 0.75$ GeV^2. The uncertainty in the overall normalization is ±3%. Figure 1 shows the ratio of the parameter A as obtained from the fits to the optical-point values derived from the total-cross-section measurements.[11] With the exception of π^-p at 50 GeV/c all values are within one standard deviation of unity, and therefore the optical point was included in the data with a 3% uncertainty. Since the measurements are consistent with other parametrizations, such as piecewise exponentials with a break at $-t = 0.15$ GeV^2 or the sum of two exponentials, the transformation to impact-parameter space has been made in numerical form and therefore in a parametrization-independent way.

The impact-parameter representation $h_{el}(s,b)$ of the elastic amplitude is defined by its Fourier transform. After integrating over the angular dependence the transformation reduces to a convolution integral of the elastic amplitude and the J_0 Bessel function. The method used to perform the transformation was to calculate, for each data point $d\sigma/dt(t_i) = d\sigma/dt_i$ and its corresponding Δt_i interval, the quantities

$$h_i(b) = \left(\frac{1}{4\pi}\right) e^{B^i_{\rm eff}|t_i|/2} \left(\frac{d\sigma}{dt_i}\right)^{1/2} \times \int_{\Delta t_i} e^{-B^i_{\rm eff}|t|/2} J_0(b\sqrt{-t})dt \,, \tag{2}$$

$$\Delta h_i(b) = \left(\frac{1}{4\pi}\right) e^{B^i_{\rm eff}|t_i|/2} \Delta\left(\frac{d\sigma}{dt_i}\right)^{1/2} \times \int_{\Delta t_i} e^{-B^i_{\rm eff}|t|/2} J_0(b\sqrt{-t})dt \,, \tag{3}$$

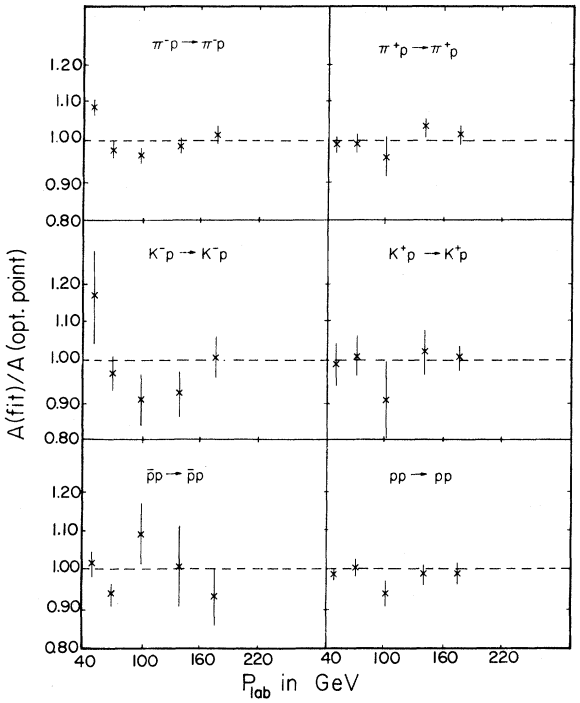

FIG. 1. The ratio of parameter A, as obtained from the fits to Eq. (1) to the optical-point values as calculated from σ_{tot} given by Ref. 11 and corrected for the real part using the results given in Ref. 2 for the elastic reactions $\pi^{\pm}p$, $K^{\pm}p$, pp, and $\bar{p}p$.

where $B^i_{\rm eff}$ is the logarithmic slope $d(\ln d\sigma/dt)/dt$ given by the parametrization (1) at the value t_i and $\Delta(d\sigma/dt_i)^{1/2}$ is the statistical error on $(d\sigma/dt_i)^{1/2}$. Finally, $h_{el}(s,b) = \sum_i h_i(b)$ and $\Delta h_{el}(s,b) = \{\sum[\Delta h_i(b)]^2\}^{1/2}$ are calculated for each b and s value and for all six reactions. The function $h_{el}(s,b)$ was found to be independent of the value taken for $B^i_{\rm eff}$, for b values smaller than 1.8 fermi. For example, by taking $5 \times B^i_{\rm eff}$ for the transformation identical results (to within 1%) for $h_{el}(s,b)$, $b \leq 1.8$ fermi, were obtained, and therefore $\Delta h_{el}(s,b)$ represents the error in the transformation.

The unitarity equation in impact-parameter space is

$$\mathrm{Im}h_{el}(s,b) = \tfrac{1}{4}\left|h_{el}(s,b)\right|^2 + G_{\rm inel}(s,b) \,, \tag{4}$$

where the different terms are related to the total, elastic, and inelastic cross sections as follows:

$$\frac{d\sigma_{\rm tot}}{\pi\, db^2} = \mathrm{Im}h_{el}(s,b) \,,$$

$$\frac{d\sigma_{\rm el}}{\pi\, db^2} = \tfrac{1}{4}\left|h_{el}(s,b)\right|^2 \,, \tag{5}$$

$$\frac{d\sigma_{\rm inel}}{\pi\, db^2} = G_{\rm inel}(s,b) \,.$$

To use Eq. (4), a knowledge of the real and imaginary parts of $h_{el}(s,b)$ is needed. Since the real part of the elastic amplitude can only be measured in the Coulomb-interference region, a model must be used to estimate the real part of $h_{el}(s,b)$.

Figure 2 shows the decomposition of $h_{el}(s,b)$ for π^+p at 50 GeV/c, as an example, into the contribution from various t regions. The main contribution comes from the region $-t \leq 0.15$ GeV^2, where in terms of the elastic amplitude $A(t)$ the measured ratios $\rho(t) = \mathrm{Re}A(t)/\mathrm{Im}A(t)$ can be used. The Coulomb-interference measurements[2] give $\rho(0) \leq 0.15$ for all processes in our energy range, and therefore the real-part contribution to $h_{el}(s,b)$ from the small $-t$ region is less than 1%. Interpreting the dip at $t = -1.4$ GeV^2 in pp elastic scattering seen at ISR energies as a zero of the imaginary part of the elastic amplitude,[3] an estimate of the real part at $t \neq 0$ can be made by using a linear extrapolation for $1/\rho(t)$ from the measured $\rho(0)$ value. In πp and Kp scattering such a dip is not seen at Fermilab[12] energies and can therefore be assumed to occur at larger $-t$ values, giving a smaller value for $1/\rho(t)$ slope. The real-part contributions to $h_{el}(s,b)$ from the regions $0.15 \leq -t \leq 0.4$ GeV^2 and $0.4 \leq -t \leq 0.75$ GeV^2 calculated by taking twice the $\rho(t)$ value predicted by the linear extrapolation are each less than 2%. The procedure is comparable to allowing the Pomeron slope to be as large as 0.6 GeV^{-2}. Finally, the different t regions contribute to $h_{el}(s,b)$ with different signs and produce a partial cancellation of the real part. Therefore, the conclusion is that the overall error in the assumption

$$\mathrm{Im}h_{el}(s,b) = |h_{el}(s,b)| \tag{6}$$

is less than 3%.

Since the impact-parameter representation of the elastic amplitude is obtained by integrating over all t values, the contributions to $h_{el}(s,b)$ from $-t \geq 0.75$ GeV^2 had to be estimated. The data taken at $P_{lab} = 100$ GeV/c extended out to $-t = 1.4$ GeV^2 and they were used to estimate the contributions from large $-t$ values at other energies. The ratio

$$\frac{h_{el}(b,\ \text{for}\ -t \leq 1.4\ \text{GeV}^2)}{h_{el}(b,\ \text{for}\ -t \leq 0.75\ \text{GeV}^2)} = 1 + C^{xp}(b) \tag{7}$$

was calculated for the reactions $pp \to pp$ and $\pi^\pm p \to \pi^\pm p$. This ratio is 1 for $b > 0.2$ fermi and is equal to 1.02 and 1.06 at $b \approx 0$ for pp and πp, respectively. Since the real part of the elastic amplitude becomes comparable to the imaginary part for $-t \geq 0.75$ GeV^2, the impact-parameter representation has been corrected by taking half of the large-$|t|$ correction:

$$\mathrm{Im}h_{el}(s,b) = h_{el}[s,b,-t \leq 0.75\ \text{GeV}^2][1 + \tfrac{1}{2}C^{xp}(b)], \tag{8}$$

where $C^{pp}(b)$ was used for pp and $\bar{p}p$, and $C^{\pi^\pm p}(b)$ was used for $\pi^\pm p$ as well as $K^\pm p$. An uncertainty of $\frac{1}{2}C^{xp}(b)$ was included for this procedure. An additional uncertainty for $b \leq 0.1$ fermi is due to the contributions from $-t \geq 1.4$ GeV^2. Because of the lack of data in meson-baryon elastic scattering at high $|t|$ in this energy range and the uncertainties in the real parts at large $|t|$ values, this correction cannot be directly determined; but it has been estimated to be less than 3% for the meson-baryon case and 1% for the baryon-baryon case.

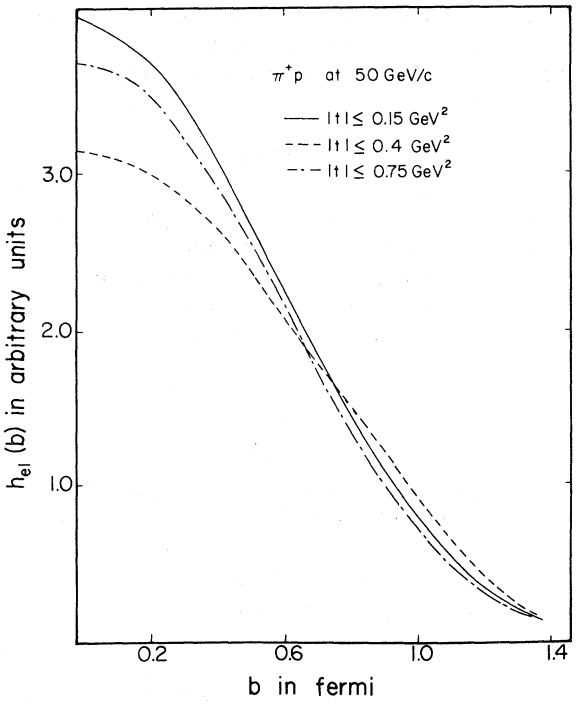

FIG. 2. $h_{el}(s,b)$ for π^+p at 50 GeV/c in arbitrary units for the integration ranges indicated.

III. GENERAL CHARACTERISTICS

Figure 3 shows the imaginary part of the elastic amplitude as defined in Eq. (8) as a function of the impact parameter for all reactions at $P_{lab} = 50$ and 175 GeV/c. The errors shown include the uncertainty in the correction for the contribution in the region $0.75 \leq |t| \leq 1.4$ GeV^2. The following conclusions can be reached: (a) $\pi^\pm p$ and $K^- p$ show almost no change as a function of energy, (b) $K^+ p$ shows a slight increase as a function of energy for all b values, (c) $\bar{p}p$ shows a slight decrease as a function of energy for all b values within the un-

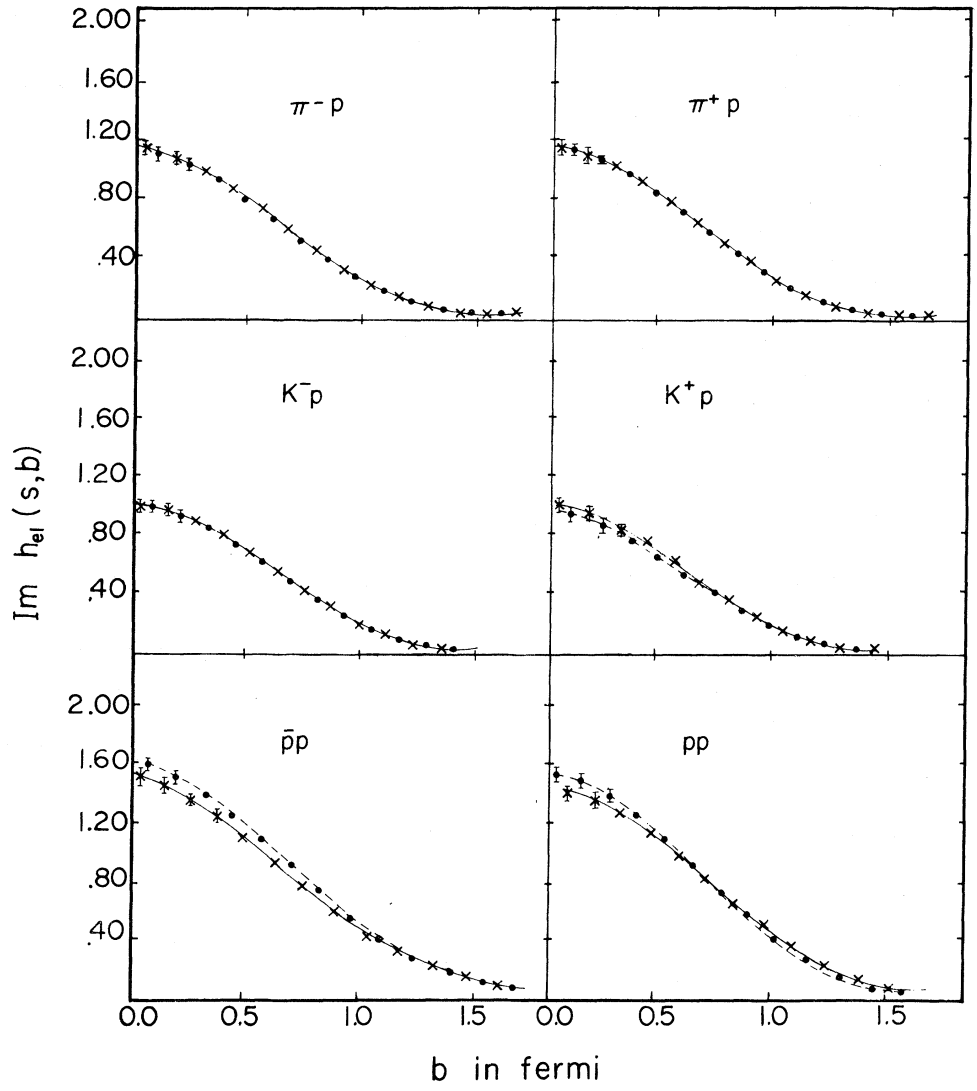

FIG. 3. $\mathrm{Im}h_{\mathrm{el}}(s,b)$ for the reactions $\pi^{\pm}p$, $K^{\pm}p$, pp, and $\bar{p}p$ at 50 GeV/c(●) and at 172 GeV/c(×). The errors shown include both the statistical errors and the uncertainty due to corrections for the large-$|t|$ contributions and the real-part effects. The errors do not include a correction for lack of data at $|t|>1.4$ GeV^2.

certainties of this analysis, and (d) in pp there is a decrease in $\mathrm{Im}h_{\mathrm{el}}(s,b)$ for small b and an increase for large b values as a function of energy.

Figure 4 shows the values of $\mathrm{Im}h_{\mathrm{el}}(s,b=0)$ as a function of s for the various processes. The errors also include the estimated error incurred by neglecting the real part of the elastic amplitude. The relative errors are much smaller since neither the real part nor the large-$|t|$ cross section changes very strongly in our energy range.

By making use of the unitarity equation (4), one can calculate the inelastic cross section $G_{\mathrm{inel}}(s,b)\equiv d\sigma_{\mathrm{inel}}/\pi\, db^2$ as a function of b. The value of this cross section at $b=0$ is shown for all processes in Fig. 5 with the full errors included as for the plots in Fig. 4. For comparison, the results of similar calculations done for pp with ISR data and a 24-GeV/c experiment[3] are included. Since $G_{\mathrm{inel}}(s,b=0)$ represents the absorption probability for a head-on collision, the results show that a baryon has a ~6% probability of colliding head-on with a proton without any absorption, while this probability is ~18% for pions and ~25% for kaons. As one can see, mesons are very transparent objects.

Figures 6(a) and 6(b) show the rms interaction

distance for the total and inelastic cross sections, defined by

$$(R_i^2)^{1/2} = \left[\int_0^{b_{\max}} b^2 \left(\frac{d\sigma_i}{db^2}\right) b\, db \Big/ \int_0^{b_{\max}} \left(\frac{d\sigma_i}{db^2}\right) b\, db \right]^{1/2} \tag{9}$$

where i = total or inelastic, and $b_{\max}$ was taken to be 1.6 fermi. For $b \geq 1.6$ fermi the impact-parameter transformation becomes very sensitive to the $d\sigma/dt$ parametrization used between $t = 0$ and the minimum $|t|$ value measured. By taking $b_{\max} = 2$ fermi, the values of $(R_{\text{tot}}^2)^{1/2}$ change by 12% for all reactions, but the results for $K^{\pm}$ and $\bar{p}$ present large fluctuations (~5%) as a function of energy. With the exception of the $\bar{p}p$ process both the total and inelastic processes are consistent with an increase in the rms interaction radius with s. The total and inelastic interaction radii for the meson-baryon interactions are 6% smaller than the baryon-baryon interaction radii.

IV. TOTAL-CROSS-SECTION INCREASE IN K^+p AND pp

The only total cross sections that show a definite increase in the energy range under study are K^+p (~7%) and pp (~1%).[11] However, when a 7% difference is spread over b space the average contribution to this difference is smaller than the error bars. Assuming that both the real parts and the large-$|t|$ contributions do not change by more than 2% within this energy range, the differences can sensibly be plotted including only the statistical errors.

Figures 7(a) and 7(b) show plots of the differences

$$\Delta\left(\frac{1}{\pi}\frac{d\sigma_{\text{tot}}}{db^2}\right)_{P_1, P_2} = \frac{1}{\pi}\frac{d\sigma_{\text{tot}}(P_1)}{db^2} - \frac{1}{\pi}\frac{d\sigma_{\text{tot}}(P_2)}{db^2} \tag{10}$$

for $P_1 = 175$ GeV/c, $P_2 = 70$ GeV/c and $P_1 = 140$ GeV/c, $P_2 = 50$ GeV/c ($P_i \equiv P_{\text{lab}_i}$) for the processes pp and K^+p, respectively. The two pairs of P_1, P_2 values were chosen in such a way that the two cross-section differences are equal[11] to within 1%, and therefore the two graphs can be compared and also averaged. The two processes appear to be different. For pp, $d\sigma_{\text{tot}}/\pi\, db^2$ is decreasing at small b values and increasing at large b values, which indicates a peripheral increase in the total cross section. For the K^+p case, the total-cross-section distribution seems to be increasing at small b values and therefore is consistent with a nonperipheral increase in the cross section.

Since this part of the analysis is speculative in nature, we have proceeded one step further to isolate the Pomeron from f exchange in impact-parameter space. This is done by looking at the SU(3) combination which isolates the ϕp total cross section:

$$\frac{d\sigma_{\text{tot}}}{\pi\, db^2}(\phi p) = \frac{d\sigma_{\text{tot}}}{\pi\, db^2}(K^+p + K^-p) - \frac{d\sigma_{\text{tot}}}{2\pi\, db^2}(\pi^+p + \pi^-p)\,. \tag{11}$$

If the f' trajectory is neglected because of its low intercept, the ϕp total cross section as defined in (11) isolates Pomeron exchange. Indeed, by taking

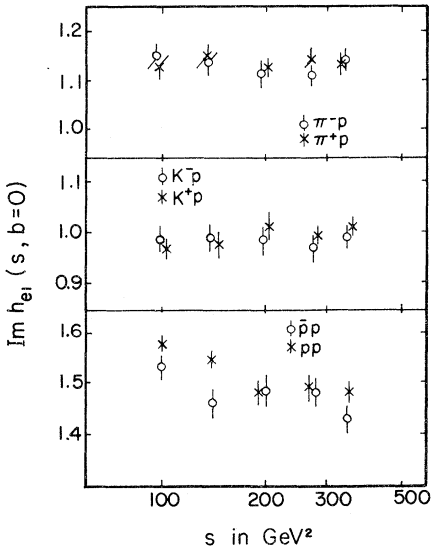

FIG. 4. $\text{Im}h_{\text{el}}(s, b=0)$ as a function of s for $\pi^{\pm}p$, $K^{\pm}p$, pp, and $\bar{p}p$. The errors are calculated as for Fig. 3.

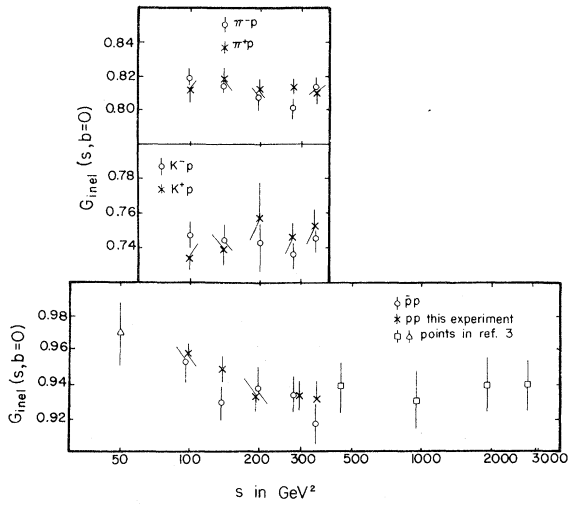

FIG. 5. $G_{\text{inel}}(s, b=0)$ as a function of s for $\pi^{\pm}p$, $K^{\pm}p$, pp, and $\bar{p}p$. The errors are calculated as for Fig. 3. The ISR and 24-GeV/c points in pp are included as given in Ref. 3.

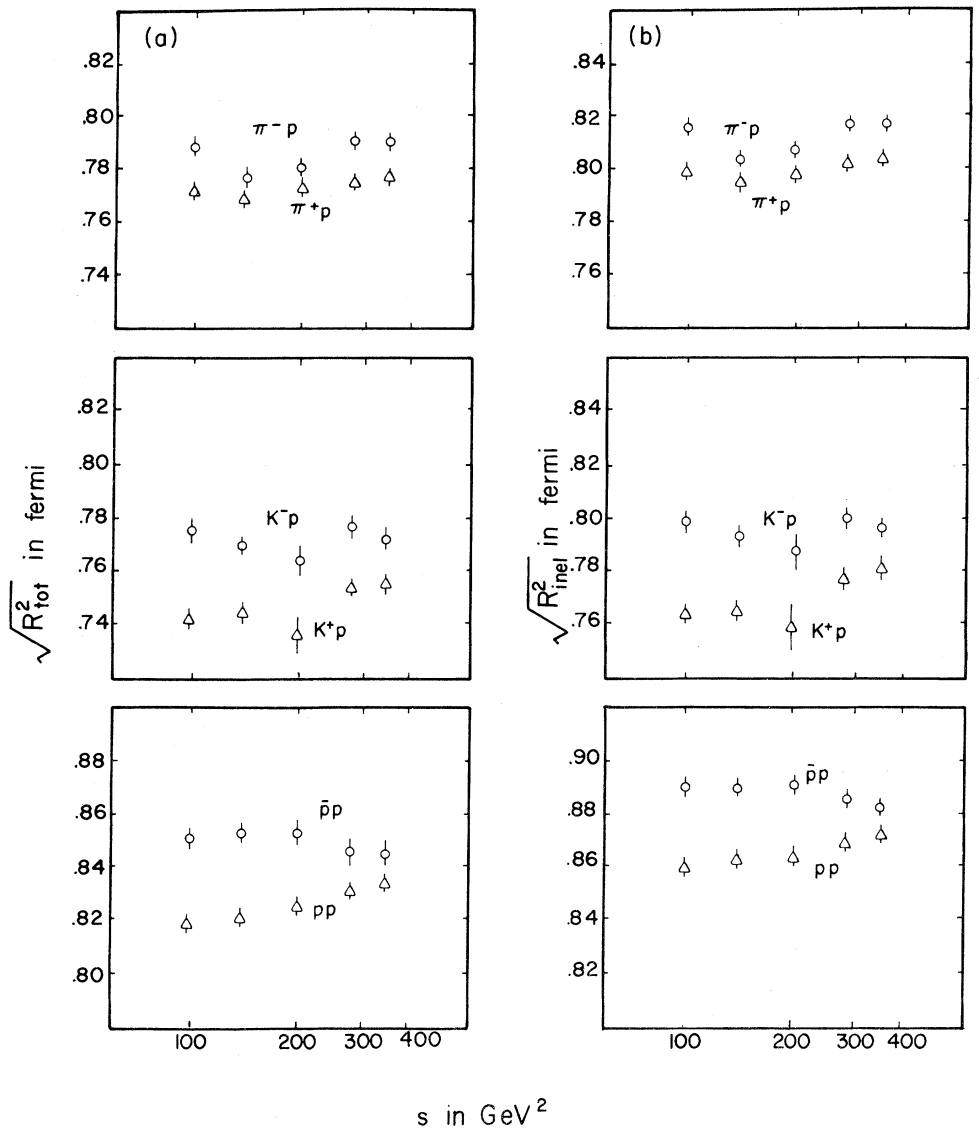

FIG. 6. The rms interaction distances for (a) the total and (b) the inelastic cross sections as a function of s for $\pi^{\pm}p$, $K^{\pm}p$, pp, and $\bar{p}p$. The errors are calculated as for Fig. 3.

the above SU(3) combination, a total cross section for ϕp is obtained that increases logarithmically[13] from $P_{\text{lab}} = 6$ GeV/c to $P_{\text{lab}} = 200$ GeV/c. In Fig. 7(b), $\Delta(d\sigma_{\text{tot}}/\pi\, db^2)$ as defined in (10) for $P_1 = 175$ and $P_2 = 70$ GeV/c is plotted for the ϕp process. In contrast to the pp case the increase in the total ϕp cross section is nonperipheral and similar to the K^+p behavior.

In Figs. 8(a) and 8(b) the differences in the inelastic cross sections are plotted for same P_1, P_2 values as before. For a comparison, the average values for the two sets of total cross-section differences in Figs. 7(a) and 7(b) have also been plotted and are shown as a dash-dot curve. Since the difference between the total and inelastic cross sections is the elastic cross section, one concludes that most of the total-cross-section decrease at small b values for pp comes from the elastic-cross-section decrease, while the large-b increase comes mainly from an increase in the inelastic cross section.

V. UPPER LIMITS ON INELASTIC DIFFRACTION

Various recent theoretical works have treated the close interdependence between elastic and inelastic diffraction.[14] Pumplin[7] has shown that s-channel unitarity combined with the assumption

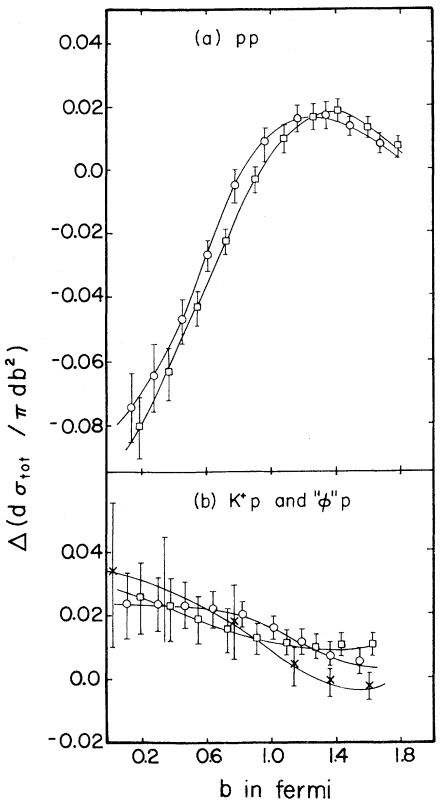

FIG. 7. $\Delta(d\sigma_{\rm tot}/\pi\, db^2)$ for pp (a) and K^+p (b) with $P_1 = 175$, $P_2 = 70$ GeV/c (○) and $P_1 = 140$, $P_2 = 50$ GeV/c (□). In (b) the difference for ϕp at $P_1 = 175$, $P_2 = 70$ GeV/c is a also plotted as (×).

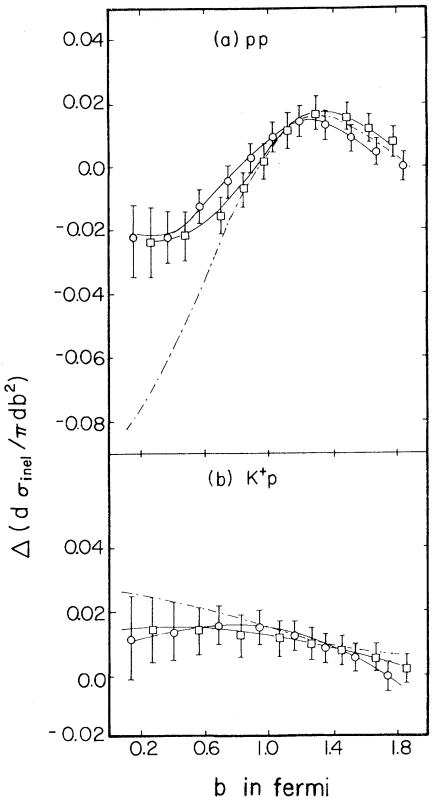

FIG. 8. $\Delta(d\sigma_{\rm inel}/\pi\, db^2)$ for pp (a) and K^+p (b) with P_1 and P_2 as in Fig. 7. The broken line is the average of the two curves presented in Fig. 7.

that inelastic as well as elastic diffraction is the shadow of nondiffractive particle production implies the following upper bound on inelastic diffraction:

$$\frac{1}{\pi}\frac{d\sigma_{\rm diff}}{db^2} \le \frac{1}{2\pi}\frac{d\sigma_{\rm tot}}{db^2} - \frac{1}{\pi}\frac{d\sigma_{\rm el}}{db^2} \equiv \sigma_{\rm diff}^{\rm max}(b)\,. \qquad (12)$$

In Fig. 9, we present a plot of $\sigma_{\rm diff}^{\rm max}(b)$ for all processes at $P = 175$ GeV/c (the plots at other energies look similar) and for comparison we plot $d\sigma_{\rm el}/\pi\, db^2$ for each reaction at 50 GeV/c and 175 GeV/c. The salient feature of those plots is that the $\sigma_{\rm diff}^{\rm max}(b)$ profile is peripheral for pp and $\bar{p}p$ in contrast to the more central meson-baryon scattering profiles. However, they are more peripheral than the corresponding elastic profiles.

Experimental results on total inelastic diffraction for pp and πp have been shown[14] to be consistent with the relation $\sigma_{\rm inel}^{\rm diff} \approx \sigma_{\rm el}$. The fact that the elastic contribution at $b = 0$ is three times the Pumplin bound for pp inelastic diffraction scattering implies that inelastic diffraction has a larger rms interaction radius than the elastic pp process. However, this is not the case for the meson-baryon process where the elastic contribution at $b = 0$ is approximately equal to the Pumplin bound, and therefore no such conclusion is possible.

VI. REGGE CONTRIBUTIONS

The crossovers between particle and antiparticle elastic cross sections for K^-p, K^+p and $\bar{p}p$, pp have been studied in lower-energy elastic-scattering experiments.[15] The crossovers have also been observed at high energies.[16] These differences have been explained in terms of dual models[10] by using the fact that K^+p and pp are exotic in the s channel so that only Pomeron exchange contributes. Further, the Regge contributions to K^-p and $\bar{p}p$ are small when compared with the Pomeron part, and only the interference term between the Pomeron term and the imaginary (Regge) term is important for the crossover. The results of these theoretical analyses[10] show that the imaginary part of the odd-charge-conjugation Regge-exchange amplitude, ω exchange in this

case, has an $e^{Bt}J_0(R\sqrt{-t})$ behavior that corresponds in impact-parameter space to a distribution peaking at $b=R$.

Presented in Figs. 10(a) and 10(b) are the differences

$$\Delta\sigma_{\text{tot}}^{xp}(b) \equiv \frac{d\sigma_{\text{tot}}(x^-p)}{\pi\, db^2} - \frac{d\sigma_{\text{tot}}(x^+p)}{\pi\, db^2} \tag{13}$$

for $x=K$ and p, respectively, at $P_{\text{lab}}=50$ and 175 GeV/c. In both cases there is an indication of a peak which decreases as a function of energy. The peak occurs at $b\approx 0.9$ fermi for Kp and $b\approx 1.2$ fermi for pp. One may conclude that the amount of nonflip ω exchange is very small in K^-p, is consistent with zero at $P_{\text{lab}}=175$ GeV/c, and is significant for $\bar{p}p$ at 50 GeV/c, but decreases very fast to a small contribution at $P_{\text{lab}}=175$ GeV/c.

VII. HADRONIC DENSITY DISTRIBUTIONS IN K, π, AND p

Chou and Yang[17] have defined a hadronic density distribution (or density of opaqueness) by assuming that the attenuation of the probability amplitude $S(b)$ for a scattering process between two hadrons is governed by the local density (opaqueness) within each hadron. In a mathematical form the above assumption for the scattering of particle a on b

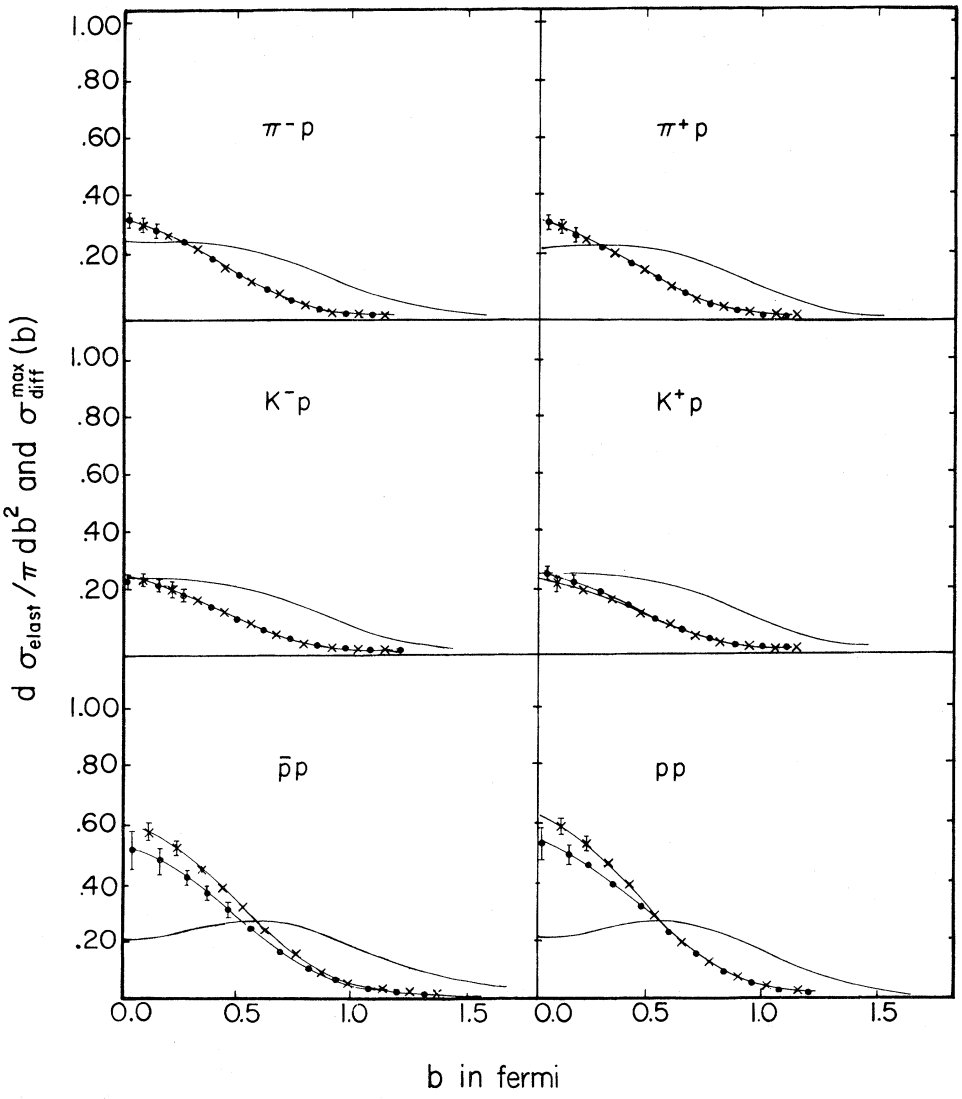

FIG. 9. $\sigma_{\text{diff}}^{\text{max}}(b)$ for $\pi^{\pm}p$, $K^{\pm}p$, and pp at $P=175$ Gev/c (solid line) and $d\sigma_{\text{el}}/\pi\, db^2$ at 50 GeV/c (×) and at 175 GeV/c (•).

would read

$$-\ln[1-\mathrm{Im}h_{el}(s,b)] = -\ln S(b) = \mathrm{Const}\times\int\int D_a(\vec{b}-\vec{b}')D_b(\vec{b}')\,db'^2\,, \tag{14}$$

where $D_i(\vec{b})$ is a two-dimension hadronic density defined by integrating the hadronic density along the direction of the incoming particle.

Denoting the Fourier transform of A by $\langle A\rangle$, then the Fourier transform of (14) would read

$$\langle -\ln[1-\mathrm{Im}h_{el}(s,b)]\rangle = \mathrm{Const}\times\langle D_a(b)\rangle\langle D_b(b)\rangle\,. \tag{15}$$

Using the pp data to determine $\langle D_p(b)\rangle$, the results can then be inserted in (14) for the πp and Kp processes to yield $\langle D_\pi(b)\rangle$ and $\langle D_K(b)\rangle$.

Chou and Yang[17] have suggested that the Fourier transform of the hadronic density should be compared with the Fourier transform of the hadronic charge distribution obtained from electron scattering measurements. Such a comparison is performed in Fig. 11 for protons and pions. In the proton case, the comparison is not well defined since the proton has two electromagnetic form factors, electric and magnetic. For that reason the comparison shown in Fig. 11(a) is done with both F_1 and G_E as obtained by Price *et al.*[18] At low energy good agreement with F_1 is experimentally obtained, while for the ISR range the agreement with G_E is better.[19] In the case of the π form factor, there are data on πe scattering only for $|t| \leq 0.04$ GeV^2 (Ref. 20), and the high-$|t|$ data points are obtained from electroproduction of pions.[21] The agreement of $\langle D_\pi(b)\rangle$ with the pion form factor, as shown in Fig. 11(b), is excellent, and therefore it is tempting to predict how the K form factor [the dash-dotted line in Fig. 11(b)] will look on the basis of this model.[22]

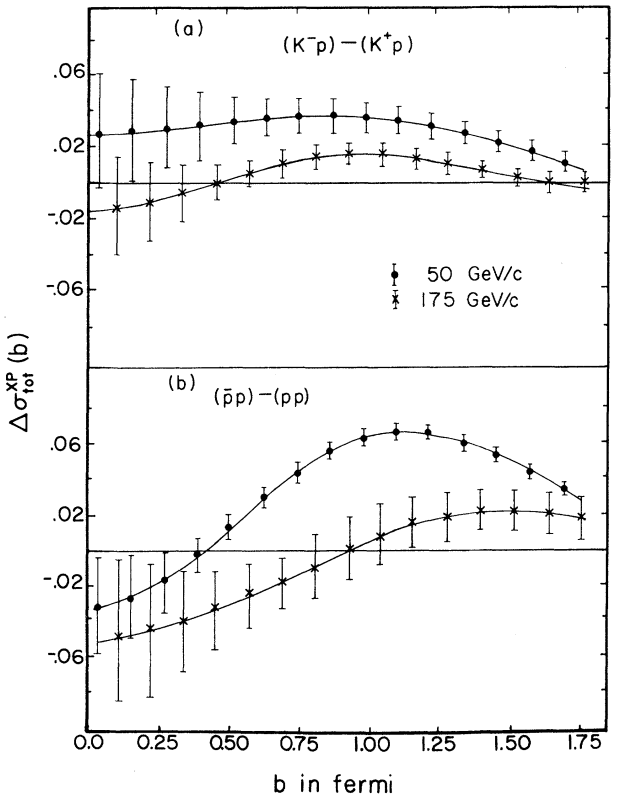

FIG. 10. $\Delta\sigma_{tot}^{xp}(b)$ for (a) Kp and (b) pp at $P=50$ GeV/c (●) and at $P=175$ GeV/c (×).

VIII. QUARK-MODEL PREDICTIONS

Various differences between meson-baryon and baryon-baryon scattering have been shown. Since

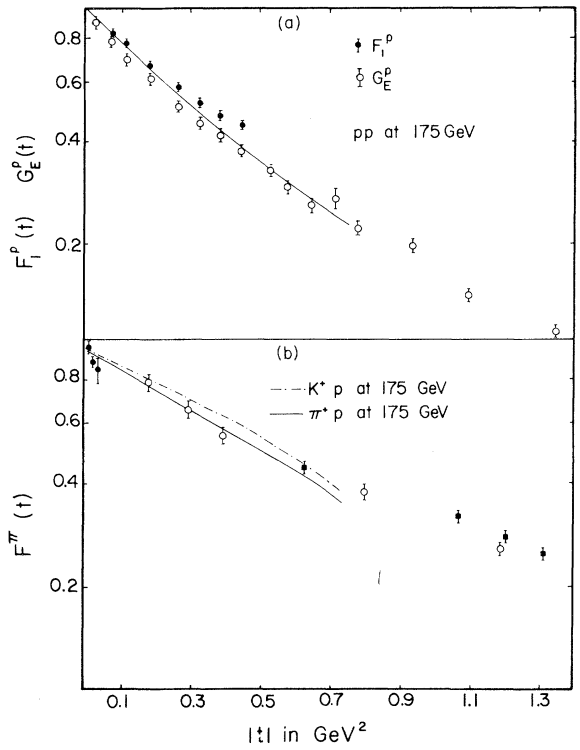

FIG. 11. (a) $F_1^p(t)$ (●) and $G_E^p(t)$ (○) proton form factors from Ref. 18. The solid line corresponds to the calculated $\langle D_p(b)\rangle$ using Eq. (14) for pp scattering 175 GeV/c, normalized to $\langle D_p(b)\rangle = 1$, at $t=0$. (b) Pion form factor measurements from Ref. 19 (●) and Ref. 20 (○,■). In the region of this measurement, the solid (dotted) line corresponds to the Fourier transform of the pion (Kaon) hadronic density calculated using (14) for π^+p (K^+p) and pp scattering at 175 GeV/c, normalized to $\langle D_\pi(b)\rangle = 1$ [$\langle D_K(b)\rangle = 1$], at $t=0$.

these processes are related in terms of quark counting in a simple quark model, a comparison between πp, Kp, and pp amplitudes in terms of those predictions will be given. Figures 12(a) and 12(b) show the differences $3/2W(\pi p) - W(pp)$ and $W(\pi p) - W(Kp)$, respectively, where

$$W(xp) = \frac{1}{2\pi}\frac{d\sigma_{\text{tot}}}{db^2}(x^+P) + \frac{1}{2\pi}\frac{d\sigma_{\text{tot}}}{db^2}(x^-p) \qquad (16)$$

for $P_{\text{lab}} = 50$ and 175 GeV/c. The prediction of quark counting is that those differences should be zero. However, owing to the facts that $\frac{3}{2}\,\text{Im}\,h_{\text{el}}^{\pi p}(s, b=0) > \text{Im}\,h_{\text{el}}^{pp}(s, b=0)$ and that the interaction radius is different for πp and pp, the difference oscillates around zero in the first case. In the second case, the fact that Kp is more transparent than πp makes the difference larger than zero. Since elastic scattering contains other exchanges besides vacuum quantum numbers, Lipkin has suggested a quark-model relation that takes into account f exchange.[23] This relation is plotted in Fig. 13, and even though it is ~7% different than unity it is quite constant for $b < 1$ fermi.

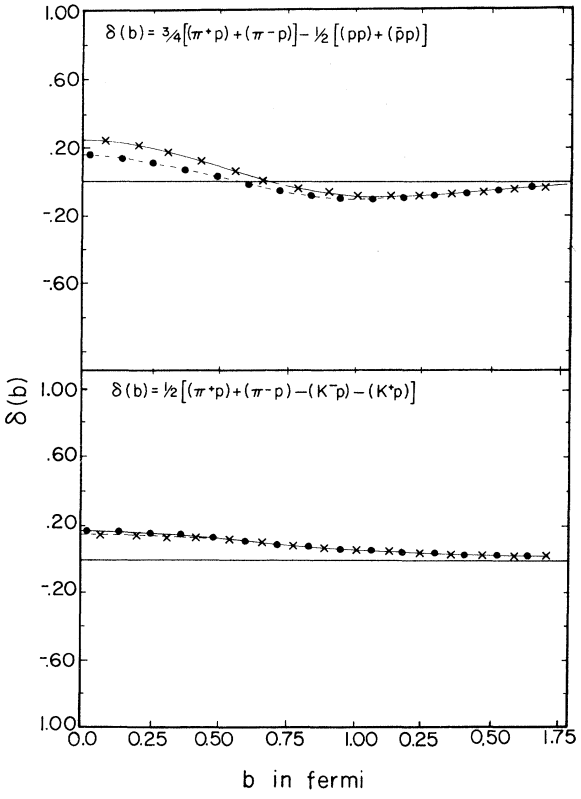

FIG. 12. Quark-model comparison at $P = 50$ GeV/c (●) and at $P = 175$ GeV/c (×).

IX. CONCLUSIONS

It has been shown that the impact-parameter representation provides a very useful tool to analyze hadronic interactions at high energies since it interrelates elastic and inelastic physics in a very natural way.

The following general conclusions can be drawn from the analysis presented on the impact-parameter representation of elastic-scattering data obtained with the Fermilab Single Arm Spectrometer:

(a) Meson-baryon interactions are ~20% more transparent than baryon-baryon interactions, which approach an opacity of 94% for $s > 200$ GeV^2.

(b) Meson-baryon processes have an interaction radius ~6% smaller than baryon-baryon processes.

(c) The decrease with energy of the $\bar{p}p$ elastic cross section at large b values ($b \sim 1$ fermi) is correlated with the decrease of $C = -1$ (nonflip ω) Regge exchanges, while the decrease at small b values is common to both pp and $\bar{p}p$ elastic cross section and is produced by a different mechanism.

(d) The increase in the pp total cross section as a function of energy is peripheral, while in the K^+p case this increase could also be central.

(e) The Pumplin upper limit for inelastic diffration requires pp and $\bar{p}p$ inelastic diffraction to be more peripheral than the elastic process, but imposes only very small restrictions in the meson-baryon case.

(f) The Fourier transform of the π hadronic density is found to be in excellent agreement with the π form factor measurements.

(g) The results of the analysis disagree with the simple quark-model counting.

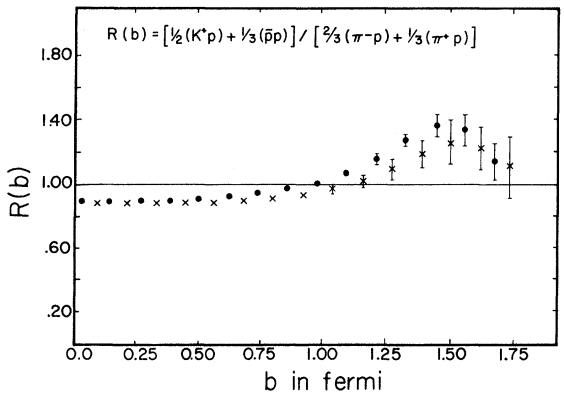

FIG. 13. Quark-model (modified for f exchange) comparison for $P = 50$ GeV/c (●) and $P = 175$ GeV/c (×).

ACKNOWLEDGMENT

We would like to thank Dr. E. Rabinovici and Dr. U. Maor for their very stimulating discussions. We would also like to express our thanks to the many people at our home institutions and at Fermilab who have contributed to the successful operation of the Single Arm Spectrometer.

---

†Work supported in part by the U. S. Energy Research and Development Administration, the National Science Foundation, and Istituto Nazionale di Fisica Nucleare, Italy.

*Current address: Daresbury Nuclear Physics Laboratory, Daresbury, Lancashire, England.

‡Also at Centre d'Etudes Nucléaire de Saclay, 91 Gif-sur-Yvette, France.

§Current address: University of Chicago, Chicago, Illinois 60637.

‖Current address: University of Utah, Salt Lake City, Utah 84112.

¶Current address: University of Illinois, Champaign—Urbana, Illinois 61801.

**Current address: Centre d'Etudes Nucléaire de Saclay, 91-Gif-sur-Yvette, France.

[1]A. Bohm *et al.*, Phys. Lett. B49, 491 (1974).

[2]V. Bartenev *et al.*, Phys. Rev. Lett. 31, 1367 (1974); U. Amaldi *et al.*, Phys. Lett. 43B, 231 (1973). See also J. Lach, Fermilab Report No. CONF-76/15 (unpublished).

[3]H. I. Miettinen, in *High Energy Hadronic Interactions*, proceedings of the IX Recontre de Moriond, 1974, edited by J. Tran Thanh Van (CNRS, Paris, 1974).

[4]R. Henzi and P. Valin, Phys. Lett. B48, 119 (1974).

[5]F. S. Henyey *et al.*, Nucl. Phys. B70, 445 (1974).

[6]A. W. Chao and C. N. Yang, Phys. Rev. D 8, 2063 (1973).

[7]J. Pumplin, Phys. Rev. D 8, 2899 (1973); see also R. Blankenbecler *et al.*, *ibid.* 9, 736 (1974).

[8]Fermilab Single Arm Spectrometer Group, Phys. Rev. Lett. 35, 1195 (1975) and D. S. Ayres *et al.*, Fermilab Report 76/66 EXP(7100.096) (unpublished).

[9]J. Butler, M.I.T., Ph.D. thesis, 1975 (unpublished); D. Cutts and B. Heltsley, Brown University Internal Reports Nos. 135 (COO-313OTB-219) and 137 (COO-313OTB-221) (unpublished); G. Mikenberg, J. Butler, and D. Cutts, Bull. Am. Phys. Soc. 21, 669 (1976).

[10]M. Davier and H. Harari, Phys. Lett. B40, 281 (1972).

[11]A. S. Carroll *et al.*, Phys. Rev. Lett. 33, 928 (1974).

[12]C. W. Akerlof *et al.*, Phys. Rev. Lett. 35, 1406 (1975).

[13]C. Quigg and E. Rabinovici, Phys. Rev. D 13, 2525 (1975).

[14]K. Fialkowski and H. I. Miettinen, CERN Report No. Th.2057, 1975 (unpublished).

[15]I. Ambats *et al.*, Phys. Rev. D 9, 1179 (1974); see also G. Brandenburg *et al.*, Phys. Lett. 58B, 367 (1975); 58B, 371 (1975).

[16]R. L. Anderson *et al.*, Phys. Rev. Lett. 37, 1025 (1976).

[17]T. T. Chou and C. N. Yang, Phys. Rev. 170, 1591 (1968).

[18]L. E. Price *et al.*, Phys. Rev. D 4, 45 (1971).

[19]A. W. Chao and C. N. Yang, Phys. Rev. D 8, 2063 (1973).

[20]G. T. Adylov *et al.*, Phys. Lett. 51B, 402 (1974).

[21]C. J. Bebek *et al.*, Phys. Rev. D 13, 25 (1976).

[22]A similar analysis was performed on preliminary data of a different elastic-scattering experiment: T. T. Chou, Phys. Rev. D 11, 2145 (1975).

[23]H. J. Lipkin, Phys. Lett. B56, 76 (1975).